

Preparation and plasmonic properties of polymer-based composites containing Ag–Au alloy nanoparticles produced by vapor phase co-deposition

H. T. Beyene · V. S. K. Chakravadhanula ·
C. Hanisch · M. Elbahri · T. Strunskus ·
V. Zaporojtchenko · L. Kienle · F. Faupel

Received: 6 February 2010 / Accepted: 26 May 2010 / Published online: 22 June 2010
© Springer Science+Business Media, LLC 2010

Abstract Nanocomposite (NC) thin films with noble metal nanoparticles (NPs) embedded in a dielectric material show very attractive plasmonic properties due to dielectric and quantum confinement effects. For single component NPs, the plasmon resonance frequency can only be tuned in a narrow range. Much interest aroused in bimetallic NPs, however, many wet chemical approaches often lead to core shell particles, which exhibit multiple plasmon resonances or do not allow large variation of the NPs alloy composition and filling factor. Here, we report a vapor phase co-deposition method to produce polymer-metal NCs with embedded homogeneous Ag–Au alloy particles showing a single plasmon resonance. The method allows production of NPs with controlled alloy composition (x), metal filling (f), and nanostructure in a protecting

Teflon AF matrix. The nanostructure size and shape were characterized by transmission electron microscope. Energy dispersive X-ray spectroscopy was used to determine x and f . The optical properties and the position of surface plasmon resonance were studied by UV–Vis spectroscopy. The plasmon resonance can be tuned over a large range of the visible spectrum associated with the change in x , f , and nanostructure. Changes upon annealing at 200 °C are also reported.

Introduction

Recently, there is much interest in nanocomposite (NC) thin films containing metallic nanoparticles (NPs) embedded in a dielectric matrix due to their novel functional properties offering hosts of new applications [1]. Particularly optical properties arising from the particle surface plasmon resonance (SPR) have been studied extensively [2]. SPRs are observed for the so-called free electron metals and, in particular, for noble metal (Au, Ag, and Cu) NPs due to the interaction of surface electrons with the electromagnetic wave and the contribution from the interband transition of the d -shell electrons. Experimental and theoretical investigations of the extinction coefficient for small spherical clusters in a non-absorbing medium were carried out using the Mie theory [3–5]. Based on this theory, the absorption peak is dependent on the type of metal, the surrounding medium, size and shape of the particles, the metal filling factor, as well as the interparticle distance. Thus, considerable effort has been devoted to tuning the optical properties of nanocomposites by varying the size, shape, metal filling factor, and refractive index of the surrounding host. However, the effects are very small in the case of monometallic NPs such as Ag, Au, and Cu.

H. T. Beyene · V. S. K. Chakravadhanula · C. Hanisch ·
M. Elbahri · T. Strunskus · V. Zaporojtchenko · F. Faupel (✉)
Faculty of Engineering, Institute for Materials Science—
Multicomponent Materials, Christian-Albrechts University
at Kiel, Kaiserstr. 2, 24143 Kiel, Germany
e-mail: fff@tf.uni-kiel.de

V. S. K. Chakravadhanula · L. Kienle
Faculty of Engineering, Institute for Materials Science—
Synthesis and Real Structure, Christian-Albrechts University
at Kiel, Kaiserstr. 2, 24143 Kiel, Germany

Present Address:
H. T. Beyene
Plasma and Materials Processing, Department of Applied
Physics, Eindhoven University of Technology, Den Dolech 2,
P.O. Box 513, 5600 MB Eindhoven, The Netherlands

Present Address:
M. Elbahri
Faculty of Engineering, Institute for Materials Science—
Nanochemistry and Nanoengineering, Christian-Albrechts
University at Kiel, Kaiserstr. 2, 24143 Kiel, Germany

Especially, Ag NPs exhibit only a weak shift in the position of the plasmon band as a result of the change in the size of the clusters due to the fact that the resonance frequency is located below the interband threshold [6].

Bimetallic (BM) NPs have attracted much interest because their properties can be very different from the particles of their constituents [7]. What makes them very attractive, either as alloys or in core–shell structures, is that their catalytic, electronic, and optical properties can vary dramatically not only due to size effects as in pure NPs but also as a result of the composition of different metals [3]. Concerning optical properties, the motivation to prepare BM NPs arose due to the ability to tune the SPR for a large range of wavelength within the two boundaries of the constituents as a result of the change in their composition. Taking into account the similarities in the electron density and the effective mass between Ag and Au, one might not expect a difference in the plasmon band position of NPs of these materials within the same surrounding host and particle size. Nevertheless, the difference in the interband transition of the *d*-electrons between Ag and Au leads to pronounced differences in the plasmon resonance position. A linear proportionality between the composition of the NPs and the SPR peak position has been reported previously [4, 8].

Various methods of synthesis exist to obtain BM NPs by both chemical and physical processes, with the major contribution coming from the chemical processes. In both techniques, BM alloy NPs can be formed directly during deposition of the constituent metals or using a two-step synthesis of the constituent metals followed by various treatments to achieve an alloy formation [9]. The two-step tandem processes are used mainly for the formation of core–shell structures. Link et al. [10] and Moskovits et al. [11] prepared Ag–Au alloy NPs by co-reduction of metal salts consisting of Au and Ag, using a reducing agent in a solution. The preparation of core–shell structures of Au and Ag by a two-step reduction of metal salts was carried out by Hodak et al. [12], and the transformation of this structure into alloyed NPs using laser-induced melting was reported by Schierhorn and Liz-Marzan [13]. Physical deposition techniques were also implemented to produce BM NPs. Papavassiliou [14] prepared BM NPs by evaporating Ag–Au alloys of the desired composition, which were initially prepared by melting and mixing both Au and Ag together in a silica crucible. Later, Ag–Au and Ag–Cu BM alloy NPs were prepared by Cottancin et al. [15] using laser-induced evaporation of an alloy target. Moreover, BM MPs were also produced by using alternative pulsed laser radiation from different targets by Gonzalo et al. [16]. The transformation of an Ag–Au core–shell structure that was prepared by using a two-step evaporation method into a completely alloyed BM structure by annealing the film at 300 °C was demonstrated by Baba et al. [17].

Recently, the wet chemical synthesis of polymer-based nanocomposites containing Ag–Au NPs was reported independently by Karthikeyan et al. [18] and Belotelov et al. [19]. Karthikeyan et al. demonstrated very interesting nonlinear optical properties. A linear proportionality between the composition of the NPs and the SPR peak position for Ag–Au alloy NPs were studied theoretically and a numerical calculation was reported previously [20].

In this work, we report a novel co-evaporation technique to produce nanocomposites containing BM Ag–Au NPs in a protecting Teflon AF fluoropolymer matrix. Unlike many wet chemical approaches, which lead to core shell particles with multiple plasmon resonances, the present approach yields homogeneous alloy NPs and allows much better control of the NPs filling factor in the polymer matrix and the NPs alloy composition. In addition, we also present the plasmonic properties over a wide composition range.

Experimental details and characterization

We prepared BM Ag–Au NPs in the polymer matrix by using simultaneous vapor phase deposition of the constituent metals and TAF from three independent evaporation sources. This extends our approach reported earlier to produce nanocomposites with monoatomic NPs [21, 22]. The deposition was done in a home made chamber with an initial base pressure of 2.4×10^{-5} Pa. A schematic of the experimental setup can be seen in Fig. 1. Two quartz crystal thickness monitors (1 & 2) were used to determine and control the deposition rate of the metals independently of each other during the experiment. The deposition rate of TAF was determined prior to the co-deposition process. The possibility to control the rate of deposition of the constituent metals independently and thickness gradient at the substrate level due to an angle deposition and symmetrical arrangement of the evaporators allow to produce BM polymer composites with well-defined *x* and *f*.

The deposition rates of the metals and the polymer were varied between 0.4–4 and 0.5–1.5 nm/min, respectively. In addition to the quartz crystal microbalance, the local deposition rate of each component was determined by using a thin shadow mask with a width of 1 mm and a thickness of 0.3 mm on the substrate. The microscopic image and the thickness profile (see Fig. 2) clearly indicate the various regions (pure Au(C), pure Ag (E), Au/Teflon (B), Ag/Teflon (F), and Ag–Au/Teflon (A and G)) near the two opposite edges of the mask (D) in a shadowed area. The film thickness measurement was carried out using a Talystep Profilometer (Dektak 8000). The local deposition rates of the constituent metals were determined by assuming that the sticking coefficients of metal on metal are unity.

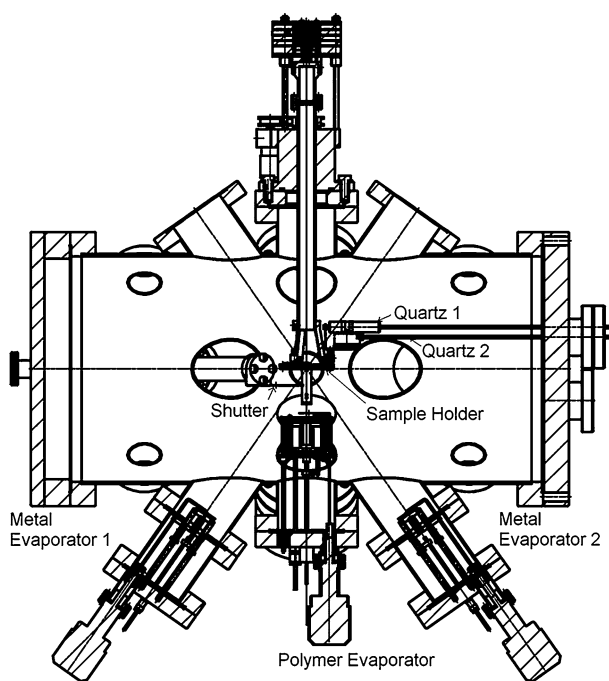


Fig. 1 Schematic of the home made deposition chamber with two quartz crystal thickness monitors and three evaporation sources

An energy dispersive X-ray spectrometer (EDX) mounted to a Philips X L30 scanning electron microscope (SEM) was used to determine the amount of each constituent metal in the composite films. These values served for the determination of x and f . The composition was estimated on the basis of the intensities of Au ($M\alpha$) and Ag ($K\alpha$) lines in the energy dispersive X-ray spectra as shown in Fig. 3 obtained from the NCs thin films and standard pure Au and Ag films with a thickness of 60 nm. It is known that the composition x of the BM NPs can be determined from the ratio of the intensity of the constituent elements [23, 24]. The estimation of the sticking coefficient of metals on polymers and the metal filling factor from the

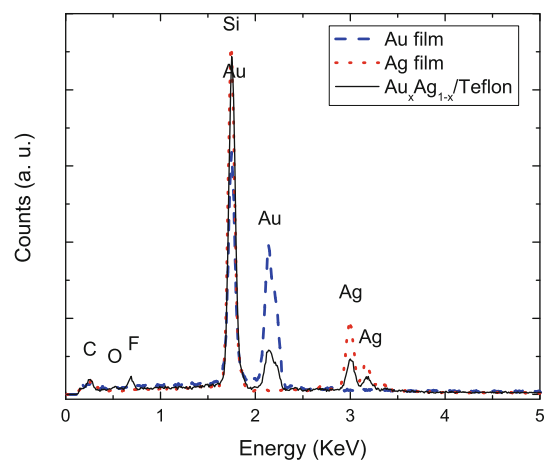


Fig. 3 EDX spectra of the nanocomposite thin film containing Ag–Au BM nanoparticles at the region (A and G) shown in Fig. 2 and standard pure Au and Ag films with a thickness of 60 nm each

atomic concentration (EDX) and thickness (Profilometer) analysis was reported in our previous articles [25, 26].

Conventional transmission electron microscopy (TEM) was carried out with a Philips CM 30 operating at 300 keV on films deposited on a carbon-coated copper grids and revealed the film morphology. High-resolution transmission electron microscopy (HRTEM) and high-angle annular dark field (HAADF)—scanning transmission electron microscopy (STEM) were carried out on Philips Tecnai F30 G² with the associated STEM–EDX analysis. Moreover, films deposited on a silicon wafer were used for X-ray photoelectron spectroscopy (XPS) analysis to confirm the BM nature of the composite films. The $\text{Ag}3d/\text{Au}4f$ peak ratio in the Ag–Au/TAF NC films is equivalent for the as-deposited and the annealed sample, which is an indication for the absence of any change in the original composition being caused by heat treatment.

The optical properties of the BM NCs were studied using a Perkin-Elmer Lambda 900 spectrometer. The

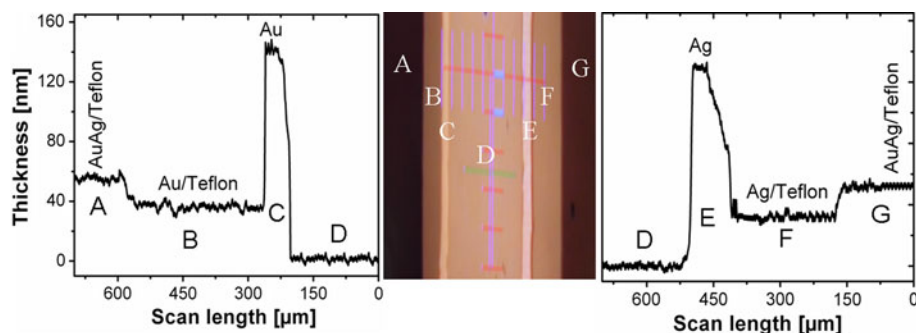


Fig. 2 Surface profiles of the film and optical microscopy image showing the regions around the two edges of the mask. The *left profile* shows the Au region (**c**) from the area exposed only to Au and masked from Ag and TAF, the Au/TAF region (**b**) from the area exposed to

Au and TAF with low angle of incident due to the middle position and masked only for Ag, and Ag–Au/TAF (**a**) from the area exposed to all evaporators. The *right profile* gives the corresponding information for Ag and **d** is the masked region

optical characterization should give the first indication on the BM alloy NPs formation. If two separate metallic phases were present, the optical absorption would be characterized by double-peaked spectra due to the SPR of single metal nanoclusters [27–29].

Results and discussion

Growth of bimetallic nanoclusters in a polymer matrix

The synthesis of BM NCs by co-evaporation takes place between highly cohesive energy metals (Ag and Au) and a low cohesive energy polymer (TAF). In addition, there is a very low interaction between the metal atoms and the polymer matrix. Therefore, various competing processes such as adsorption and reemission of metal atoms and molecules, surface diffusion, nucleation, and agglomeration have to be taken into account to understand the NPs formation in the polymer matrix [30, 31]. The large difference in thickness (more than an order of magnitude) between pure metal films around the mask and the composite film (as shown in Fig. 2) is an indication for the low sticking or condensation coefficient of metal adatoms on the polymer surface [32].

The condensation coefficient of metals on the polymer surface is very low for metals of low reactivity, as reported in our previous results [33], and depends on the rate of deposition of the metal and the type of material. Condensation coefficients of 0.2 and 0.6% were reported for Ag and Au, respectively, on a Teflon surface. However, this value increases to 10–30% in the case of co-evaporation [34]. In co-evaporation, the polymer is deposited either by evaporation of the monomers and polycondensation on the substrate or—as in the present case—by thermal cracking of suitable polymers such as TAF and repolymerization of the fragments on the substrate. In this case, the condensation coefficient of single metal adatoms is strongly dependent on the rate of growth of the polymer matrix. Compared to the co-evaporation of a single metal and a polymer, the present synthesis of BM NPs using co-evaporation of two metals along with the polymer is more complex. The condensation coefficient of one metal not only depends on its rate of deposition and the type of polymer but also on the rate of deposition of the constituent metal. Figure 4a shows that the BM composition x changes linearly with an increase in the ratio between the rate of deposition of Au and Ag at a fixed deposition rate of TAF (0.1 nm/min). In addition, the condensation coefficient of Ag is observed to increase with the change in Au composition as shown in Fig. 4b. This is due to the strong interaction of two metal atoms.

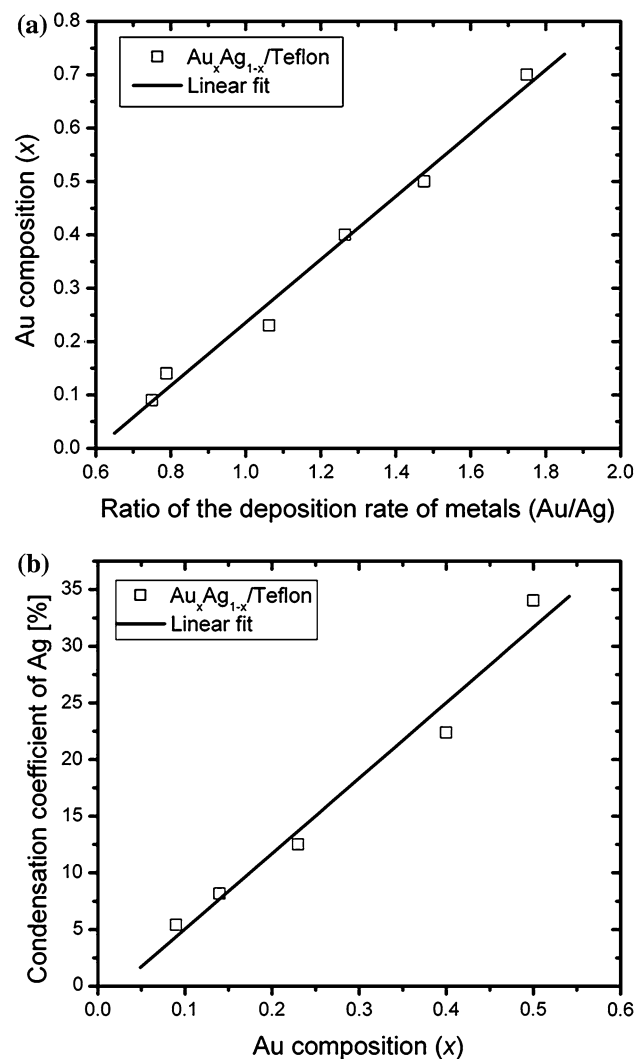
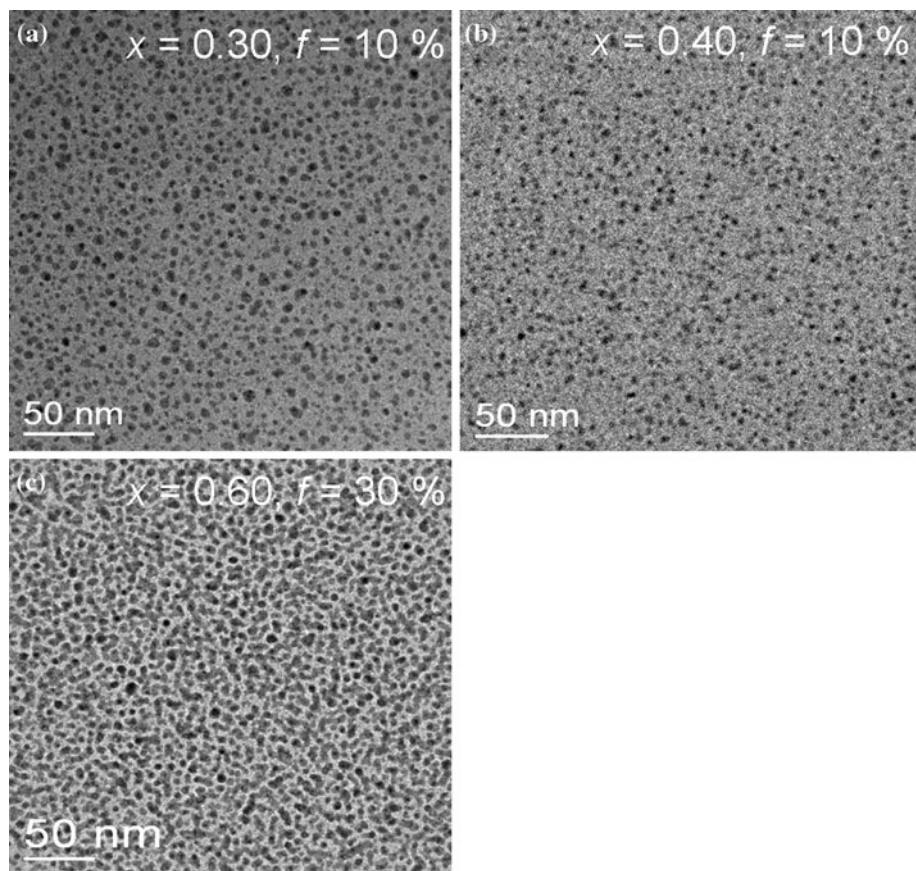


Fig. 4 The Au composition x as function of the ratio of the rate of deposition of Au to Ag (a) and the Ag condensation coefficient versus the Au composition (b)

When energetic metal atoms impinge on a polymer surface, the arriving atoms undergo various processes such as a random walk on the surface, diffusion into the polymer, or desorption [35]. Within their diffusion distance, metal atoms may encounter each other or be captured by a surface site, which both leads to nucleation, growth, and formation of stable metal clusters. Therefore, in addition to the collision energy and the sticking coefficient, the rates of nucleation and growth are determined mainly by the probability of the collisions between adatoms, between an atom and a nucleus, and between two or more nuclei.

Figure 5 shows the conventional TEM images of $\text{Ag}(\text{Au})_x/\text{TAF}$ NCs upon the variation of the amount of Au and the filling factors. The NC films synthesized by simultaneous evaporation of metals and polymer show a morphology in which the BM NPs are uniformly dispersed

Fig. 5 a–c Conventional TEM micrographs of bimetallic Ag–(Au)_x/TAF nanocomposites at various Au compositions and metal filling factors as indicated



and stably fixed in a polymer matrix. Figure 6a shows the HRTEM micrograph of the Fig. 5a with a fast Fourier transformed image displaying the *d*-spacing of (111) Au/Ag. Additionally, the HAADF–STEM image depicted in Fig. 6b shows the BM NPs of the same in Fig. 6a or 5a. Despite the appearance of the BM NPs with nearly uniform contrast in the HAADF–STEM image of Fig. 6b, the difference in contrast of some parts of the BM NPs is as a result of the overlapping BM NPs in the NC film. The polymer matrix involved in this NC prevents the detailed mapping of the sample in STEM mode because of the beam damage to the polymer matrix. The nanoprobe–EDX in STEM mode on a BM NPs confirms the presence of 66 at.% of Ag and 34 at.% of Au.

We note that while the filling factor *f* and the alloy composition of the NPs can be controlled independently, there is a correlation between NPs size and *f* in the vapor phase co-deposition method, which makes it difficult to control the two parameters independently. However, the deposition temperature may be used as an additional parameter [36].

Plasmonic properties of bimetallic-polymer nanocomposites

Figure 7 shows the plasmonic properties of the Ag–(Au)_x/TAF NCs as a function of Au composition. The sharp SPR

bands are caused by the collective oscillations of the conduction electrons due to an interaction of the electromagnetic wave with the NPs³. If the NPs are sufficiently small ($2R \ll \lambda$), the scattering becomes negligible and the absorption is equivalent with the extinction (absorption + scattering). In noble metals, the Drude electron excitation is hybridized with interband transitions, and hence the SPR shifts down to the visible region of the spectrum unlike to a free Drude metal with the same s-electron density.

It is known that due to the variation in the interband transition between Ag and Au, the SPR peaks are located at about 400 nm for Ag and about 520 nm for Au. Thus, the two plasmon bands would be expected from Ag–Au if phase separation would occur in the NPs. However, the UV–Vis extinction spectra for Ag–(Au)_x NPs (Fig. 7) shows a single plasmon band, which is expected for a homogeneous solid solution of Ag and Au in accord with the bulk phase diagram. One notes a large red shift of the plasmon peak maximum position by more than 130 nm with increasing *x*. The origin of the shift in the plasmon peak position with the change in *x* is due to the continuous change of the *d*-band energy level that contributes to the interband transition term in the dielectric function as a result of an increase in Au composition. In most of the cases, the alloy dielectric function is expressed in the form $\epsilon(x, \omega) = x\epsilon_{\text{Au}}(\omega) + (1 - x)\epsilon_{\text{Ag}}(\omega)$ [37].

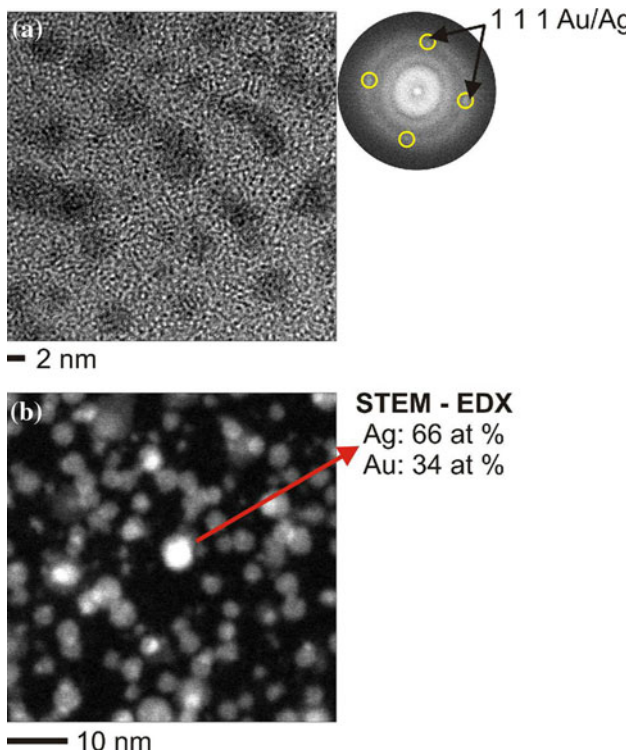


Fig. 6 **a** HRTEM micrograph with an FFT image and **b** HAADF-STEM image with a nanoprobe-EDX of Ag–(Au)_x/TAF nanocomposite of Fig. 5a

In addition to the shift in the plasmon peak position, a damping of the absorbance of the BM-polymer composites with an increase in Au composition is seen in Fig. 7. The damping minimum is close to $x = 0.5$ and is attributed to the increased electron scattering by foreign atoms upon alloying, which results in the damping of the SPR band of the pure metal [38, 39]. The disorder has a maximum for $x = 0.5$. For the higher filling factors an increase in the absorption and a large shift of the plasmon band toward the higher wavelength is observed due to the increase in particle size and the interaction between the particle plasmon resonances of neighboring particles [40, 41].

In this work, we propose an additional contribution to the intensity increase and the broadening near $x = 0.5$. We suggest that these phenomena are not only determined by the well-known factors like size and shape effects, but also influenced by a competition between the plasmon excitation and the $d-sp$ interband transition (for Au at 450–500 nm, for Ag at 300–320 nm) preventing the efficient plasmon oscillation. At low Au concentration, the plasmonic peak from the BM Ag is located near $\lambda = 420$ nm and remains at a position far away from the competition between the plasmon excitation and $d-sp$ interband transition of gold NPs and silver. However, upon increasing the amount of Au, a red shift toward the gold $d-sp$ interband transition occurs and a reduction of the plasmon peak intensity is observed. A

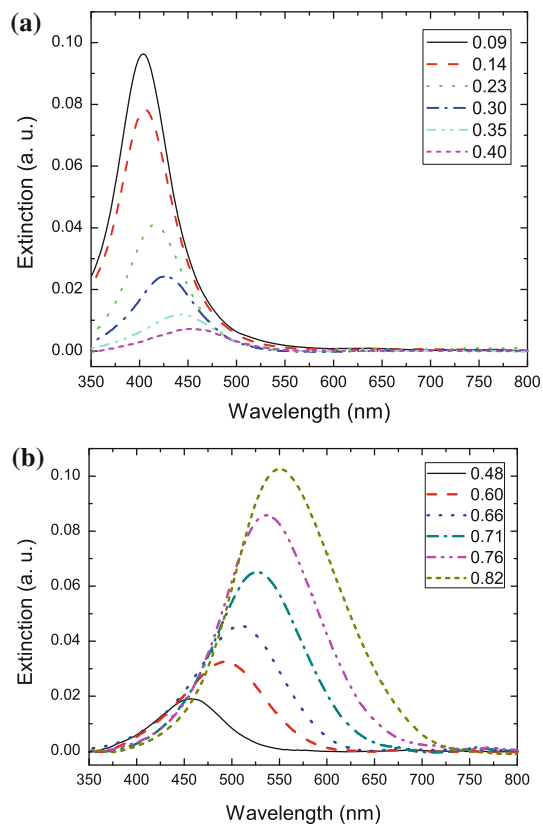


Fig. 7 Extinction spectra of TAF nanocomposites (thickness 50–70 nm) containing BM Ag–(Au)_x NPs as function of Au composition; **a** for $x < 0.45$ and **b** for $x > 0.45$. The filling factor is 10% from $x = 0.1$ to $x = 0.4$. Above $x = 0.4$, f gradually increases to higher values ($f = 30\%$ for $x = 0.6$ and $f = 40\%$ for $x = 0.86$)

further increase in the amount of gold leads to a shift in plasmon band away from the $d-sp$ interband transition toward higher wavelengths. Accordingly, efficient plasmon oscillation along with increase in the intensity is observed.

Upon annealing at 200 °C, only a slight shift of the single SPR band is observed at low filling factor (black and red curves in Fig. 8). This further confirms that a homogeneous solid solution of Ag and Au was obtained already during deposition. The slight shift in the position of the SPR band toward longer wavelength is due to the change in the size of NPs as a result of cluster growth upon annealing [36]. This effect is much more pronounced at higher filling factor (green dash and blue dash dot curves in Fig. 8) due to the shorter cluster separation. Coalescence of growing clusters with a sufficiently short separation gives rise to a strong peak broadening.

Conclusion

This article reports a new approach for better control of size, alloy composition, and metal filling factor of BM NPs

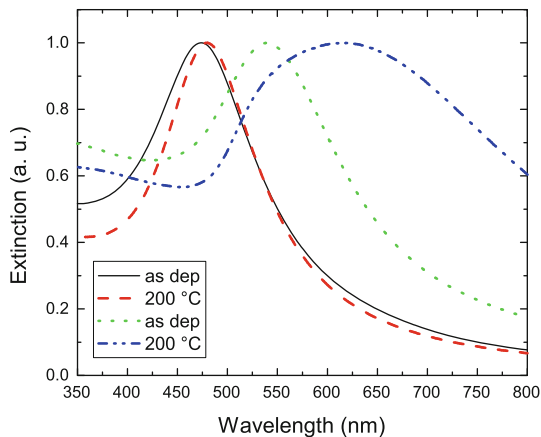


Fig. 8 UV–Visible spectra of $\text{Ag}-(\text{Au})_x/\text{TAF}$ nanocomposites (thickness $\sim 60 \text{ nm}$) for as-deposited and heat treated samples. The Au composition and metal filling are 0.16 and 48% (for solid line) and 0.82 and 48.5% (for doted line), respectively

in polymer films based on vapor phase co-deposition. The key factors are the deposition rate of the metals and of the polymer precursor. For miscible alloy systems, the method allows formation of homogeneous alloy particles directly upon deposition. Using this method, the plasmonic properties of BM $\text{Ag}-(\text{Au})_x$ NPs in a Teflon AF matrix were varied over a wide range. A single SPR peak shifting to longer wavelength with an increase in Au composition was observed. Alloying leads to an increased damping with minimum at about $x = 0.5$. The annealing behavior further confirms the formation of homogeneous alloy particles already upon deposition and reflects particle growth.

Acknowledgements We acknowledge the financial support of the German Research Foundation (DFG) under grant number Fa 234/8-1. The authors are grateful to S. Rehders for constructing the deposition chamber and for his expertise in solving technical problems.

References

1. Faupel F, Zaporjchenko V, Strunkus T, Greve H, Schurmann U, Takele H, Hanisch C, Chakravadhanula VSK, Na Ni, Gerber A, Quandt E, Podschun R (2008) Polym Polym Compos 16(8):471
2. Pinchuk AO, Schatz GC, Reinholdt A, Kreibig U (2007) Nanotechnol Res J 1:1
3. Kreibig U, Vollmer M (1995) Optical properties of metal clusters. Springer, Berlin
4. Link S, El-Sayed MA (1999) J Phys Chem B 103:8410
5. Treguer M, de Cointet C, Remita H, Khatouri J, Mostafavi M, Amblard J, Belloni J (1998) J Phys Chem B 102:4310
6. Gaudry M, Lerme J, Cottancin E, Pellarin M, Vialle JL, Broyer M, Prevel B, Treilleux M, Melinon P (2001) Phys Rev B 64:085407
7. Shibata T, Bunker B, Zhang Z, Meisel D, Vardeman C, Daniel Gezelter J (2002) J Am Chem Soc 124:11989
8. Chen D-H, Chen C-J (2002) J Mater Chem 12:1557
9. Wang C, Peng S, Chan R, Sun S (2009) Small 5:567
10. Link S, Wang ZL, El-Sayed MA (1999) J Phys Chem B 103:3529
11. Moskovits M, Srnova-Sloufova I, Vlckova B (2002) J Chem Phys 116:10435
12. Hodak JH, Henglein A, Giersig M, Hartland GV (2000) J Phys Chem B 104:11718
13. Schierhorn M, Liz-Marzan LM (2002) NanoLett 2:13–16
14. Papavassiliou GC (1976) J Phys F Metal Phys 6:L103
15. Cottancin E, Lerme J, Gaudry M, Pellarin M, Vialle J-L, Broyer M (2000) Phys Rev B 62:5179
16. Gonzalo G, Babonneau D, Afonso CN, Barnes J-P (2004) J Appl Phys 96:5163
17. Baba K, Okuno T, Miyagi M (1993) Appl Phys Lett 62:437
18. Karthikeyan B, Anija M, Philip R (2006) Appl Phys Lett 88:053104
19. Belotelov VI, Carotenuto G, Nicolais L, Longo A, Pepe GP, Perlo P, Zvezdin AK (2006) J Appl Phys 99:044304
20. Sanchez-Ramirez JF, Pal U, Nolasco-Hernandez L, Mendoza-Alvarez J, Pescador-Rojas JA (2008) J Nanomater 2008:Article ID 620412
21. Biswas A, Márton Z, Kruse J, Kanzow J, Zaporjchenko V, Faupel F, Strunkus T (2003) NanoLett 3(1):69
22. Biswas A, Aktas OC, Schürmann U, Saeed U, Zaporjchenko V, Strunkus T, Faupel F (2004) Appl Phys Lett 84(14):2655
23. Shi H, Zhang L, Cai W (2000) J Appl Phys 87:1572
24. Agrawal VV, Mahalakshmi P, Kulkarni GU, Rao CNR (2006) Langmuir 22:1846
25. Schürmann U, Hartung WA, Takele H, Zaporjchenko V, Faupel F (2005) Nanotechnology 16:1078
26. Takele H, Schürmann U, Greve H, Parekar D, Zaporjchenko V, Faupel F (2006) Eur Phys J Appl Phys 33:83
27. Mulvaney P (1996) Langmuir 12:788
28. Sun Y, Wiley B, Li Z-Y, Xia Y (2004) J Am Chem Soc 126:9399
29. Mallin MP, Murphy CJ (2002) NanoLett 2:1235
30. Faupel F, Zaporjchenko V, Strunkus T, Erichsen J, Dolgner K, Thran A, Kiene M (2000) Metallization of polymers 2 (ACS Symp. Series). Academic/Plenum, New York, p 73
31. Faupel F, Willecke R, Thran A (1998) Mater Sci Eng 22:1
32. Thran A, Kiene M, Zaporjchenko V, Faupel F (1999) Phys Rev Lett 82:1903
33. Zaporjchenko V, Zekonyte J, Biswas A, Faupel F (2003) Surf Sci 300:532
34. Takele H, Greve H, Pochstein C, Zaporjchenko V, Faupel F (2006) Nanotechnology 17:3499
35. Faupel F, Zaporjchenko V, Thran A, Strunkus T, Kiene M (2004) Metal diffusion in polymers and on polymer surfaces, Chap 7. William Andrew, Norwich, p 333
36. Takele H, Kulkarni A, Jebril S, Chakravadhanula VSK, Hanisch C, Strunkus T, Zaporjchenko V, Faupel F (2008) J Phys D Appl Phys 41:125409
37. Teo BK, Keating K, Kao Y-H (1987) J Am Chem Soc 109:3494
38. Wei SH, Mbaye AA, Ferreira LG, Zunger A (1987) Phys Rev B 36:4163
39. Murani AP (1974) Phys Rev Lett 33:91
40. Sancho-Parramon J (2009) Nanotechnology 20:235706
41. Wormeester H, Stefan Kooij E, Poelsema B (2008) Phys Status Solidi A 205:756